© 2017. Published by The Company of Biologists Ltd | Development (2017) 144, 3957-3967 doi:10.1242/dev.157917

STEM CELLS AND REGENERATION

RESEARCH ARTICLE

Rho differentially regulates the Hippo pathway by modulating the interaction between Amot and Nf2 in the blastocyst

Xianle Shi[1], Zixi Yin[1], Bin Ling[1], Lingling Wang[1], Chang Liu[1], Xianhui Ruan[2], Weiyu Zhang[1] and Lingyi Chen[1,*]

ABSTRACT

The Hippo pathway modulates the transcriptional activity of Yap to regulate the differentiation of the inner cell mass (ICM) and the trophectoderm (TE) in blastocysts. Yet how Hippo signaling is differentially regulated in ICM and TE cells is poorly understood. Through an inhibitor/activator screen, we have identified Rho as a negative regulator of Hippo in TE cells, and PKA as a positive regulator of Hippo in ICM cells. We further elucidated a novel mechanism by which Rho suppresses Hippo, distinct from the prevailing view that Rho inhibits Hippo signaling through modulating cytoskeleton remodeling and/or cell polarity. Active Rho prevents the phosphorylation of Amot Ser176, thus stabilizing the interaction between Amot and F-actin, and restricting the binding between Amot and Nf2. Moreover, Rho attenuates the interaction between Amot and Nf2 by binding to the coiled-coil domain of Amot. By blocking the association of Nf2 and Amot, Rho suppresses Hippo in TE cells.

KEY WORDS: Rho, Hippo, Amot, Nf2, F-actin, Blastocyst, Mouse

INTRODUCTION

The first cell fate decision during embryogenesis results in the segregation of the inner cell mass (ICM) and the trophectoderm (TE) in the blastocyst (Cockburn and Rossant, 2010; Zernicka-Goetz et al., 2009; Chen et al., 2010). ICM cells further differentiate into the epiblast and the primitive endoderm (PE). The epiblast give rise to the fetus, while the PE, together with the TE, contributes to the placenta.

The Hippo pathway, the core components of which are the kinases Mst1/2 and Lats1/2, and the downstream effector Yap, is involved in a wide range of biological processes, such as cell proliferation, cell death, cell differentiation, organ size control, tissue homeostasis and cancer development (Pan, 2010; Yu et al., 2015; Yu and Guan, 2013). It has been demonstrated that the Hippo pathway also regulates the differentiation of the ICM and the TE (Nishioka et al., 2009; Lorthongpanich et al., 2013). In outside TE cells of the blastocyst, Hippo signaling is repressed, and the unphosphorylated downstream effector Yap is transported into the nucleus. Consequently, Yap cooperates with Tead4 to activate the expression of transcription factor genes essential for TE development, such as *Cdx2* and *Gata3* (Nishioka et al., 2009; Yagi et al., 2007; Nishioka et al., 2008; Ralston et al., 2010). In inside ICM cells, Hippo signaling is activated and phosphorylates Yap, resulting in cytoplasmic retention of Yap. Thus, *Cdx2* cannot be activated by Tead4 in the ICM (Nishioka et al., 2009).

How the Hippo pathway is differentially regulated in TE and ICM cells of the blastocyst is a fundamental issue for understanding the first cell fate determination event. In other biological systems, cell polarity, cell adhesion, cell contact and mechanical cues have been shown to be upstream regulators for the Hippo pathway (Yu et al., 2015). Coincidently, TE cells in the blastocyst are polarized, whereas ICM cells are apolar (Thomas et al., 2004; Plusa et al., 2005; Zernicka-Goetz et al., 2009). Tight junctions are formed at the apicolateral cell contact region among polarized TE cells, whereas other cell contacts within the embryo are mediated by adherens junctions (AJs) (Sheth et al., 2000; Fleming et al., 1989; Sheth et al., 1997). The difference in cell polarity and cell adhesion between TE and ICM cells might contribute to the differentially regulated Hippo signaling. In support of this view, it has been shown that downregulation of polarity molecules, such as Par3, Par6 and atypical PKC (aPKC), leads to cytoplasmic distribution of Yap and reduced expression of Cdx2 in the TE, consequently suppressing TE formation and promoting ICM specification (Alarcon, 2010; Hirate et al., 2013; Plusa et al., 2005). Inhibition of Rho-ROCK signaling disrupts the apical-basal polarity and activates Hippo signaling (Kono et al., 2014). In addition, the junction-associated proteins angiomotin (Amot) and angiomotin-like 2 (Amotl2) mediate the signaling of cell polarity and AJs to modulate the Hippo pathway. In apolar ICM cells, the association of Amot with AJs activates the Hippo pathway. In contrast, in polarized TE cells, Amot is restricted to the apical region and absent in basolateral AJs, thereby failing to activate Hippo signaling. The phosphorylation of Amot at S176 (S175 for human AMOT) plays a crucial role in Amot binding to AJs and subsequent activation of Hippo signaling (Hirate et al., 2013; Leung and Zernicka-Goetz, 2013). Another upstream activator of the Hippo pathway, Nf2/Merlin, which is randomly distributed in the plasma membrane regions of both ICM and TE cells, is required for the activation of Hippo signaling in ICM cells (Cockburn et al., 2013), implying that suppression of Nf2 activity is necessary for TE cells to inactivate the Hippo pathway. Yet how Nf2 is repressed in TE cells, and how cell polarity, Rho-ROCK, Amot and Nf2 cooperate to regulate the Hippo pathway in the blastocyst remain to be explored.

To understand the regulatory mechanisms of the Hippo pathway in preimplantation embryos, we screened a mini-library of inhibitors and activators for signaling pathways, and identified Rho-ROCK signaling as a Hippo repressor in TE cells and PKA as a Hippo activator in ICM cells. We further demonstrated that the repressive effect of Rho on Hippo signaling is independent of cytoskeleton and cell polarity. Rather, active Rho prevents the phosphorylation of S176 in Amot, stabilizing the association between Amot and

[1]State Key Laboratory of Medicinal Chemical Biology, Key Laboratory of Bioactive Materials, Ministry of Education, Collaborative Innovation Center for Biotherapy, Tianjin Key Laboratory of Protein Sciences, 2011 Collaborative Innovation Center of Tianjin for Medical Epigenetics and College of Life Sciences, Nankai University, Tianjin 300071, China. [2]Department of Thyroid and Neck Tumor, Tianjin Medical University Cancer Institute and Hospital, National Clinical Research Center for Cancer, Key Laboratory of Cancer Prevention and Therapy, Tianjin, Huanhuxi Road, Ti-Yuan-Bei, Hexi District, Tianjin 300060, China.

*Author for correspondence (lingyichen@nankai.edu.cn)

L.C., 0000-0002-3695-3407

Received 30 July 2017; Accepted 20 September 2017

Development (2017) 144, 3957-3967 doi:10.1242/dev.157917

filamentous actin (F-actin). Meanwhile, Rho competes with Nf2 and binds to the coiled-coil (CC) domain of Amot. Consequently, sequestering Amot from Nf2 secures the inactive status of Hippo signaling in TE cells. Our results reveal a novel mechanism by which Rho can regulate Hippo signaling.

RESULTS

Identification of Rho and PKA as regulators for Hippo signaling in the blastocyst

To search for upstream regulators of the Hippo pathway in the morula and the blastocyst, a small-scale screening was carried out with a mini-library of inhibitors and activators for signaling pathways that are known Hippo regulators or crucial for preimplantation development. To avoid inhibitor- or activator-induced developmental defects, which might perturb proper Hippo regulation, a short-time (2 h) exposure to inhibitors or activators was performed with late stage morula and early stage blastocysts. To read out the status of the Hippo pathway, the subcellular distribution of Yap was examined in control and treated embryos by immunofluorescence staining. Okadaic acid (OA), an inhibitor for protein phosphatase 1 and 2A (PP1 and PP2A), was used as a control, because of its activation effect on the Hippo pathway (Hata et al., 2013). Similar to OA, inhibitors targeting the Rho-ROCK signaling, including C3 transferase (C3) and CCG1423, and Y27632 promote cytoplasmic localization of Yap in TE cells. Meanwhile, these treatments lead to blastocoel collapse (Fig. 1A-C). Conversely, Yap is localized to the nucleus of ICM cells upon PKA inhibition (Fig. 1A, Fig. S1F).

We were particularly interested in the regulatory effect of Rho-ROCK signaling on the Hippo pathway, because it is also important for early embryo development (Clayton et al., 1999). To ensure the regulatory effect of Rho on the Hippo pathway, we tested whether overexpression of constitutively active RhoA (caRhoA) rescues the mislocalization of Yap in C3-treated embryos. Glutamine 63 in the switch II region of RhoA is replaced with a leucine to mimic the deamidation status, thus leading to constitutive activation of RhoA and resistance to C3 transferase (Vogelsgesang et al., 2007). mRNAs encoding caRhoA and H2B-mCherry were injected into one blastomere of the two-cell embryo. At the late morula stage, embryos were treated with C3 for 2 h. Expression of caRhoA leads to the nuclear localization of YAP in ICM cells. More importantly, the nuclear localization of Yap is maintained in blastomeres expressing caRhoA, even after C3 treatment (Fig. 1D). We then asked whether the activity of Rho is differentially regulated in the blastocyst. As demonstrated by Rho-GTP affinity assay, active Rho (Rho-GTP) is enriched at the apical region of TE cells and is almost undetectable in the ICM (Fig. 1E). Consistently, apical enrichment of Rho-GTP is demonstrated by immunofluorescence staining with an antibody specifically recognizing active RhoA (Fig. 1F). These data indicate that Rho signaling suppresses the Hippo pathway in the TE, and that lack of Rho activity in the ICM leads to the activation of Hippo.

Rho-mediated inhibition of Hippo signaling does not require cytoskeleton remodeling or cell polarity disruption

It has been proposed that Rho GTPases, modulated by G-protein coupled receptors (GPCRs) and mechanical cues, including cell contacts and cell attachment status, remodel the cytoskeleton to regulate Hippo signaling (Zhao et al., 2012, 2007; Yu et al., 2012, 2015). To test whether Rho inhibits Hippo signaling through modulating the organization of F-actin and/or microtubules, we first examined the organization of F-actin and microtubules after C3 treatment, and found that C3 treatment has a negligible effect on cytoskeleton organization in embryos (Fig. 2A,B). Next, we treated embryos with chemicals that altered actin or microtubule dynamics. To our surprise, actin polymerization inhibitors, cytochalasin D (CCD) and latrunculin B (LatB), do not activate the Hippo pathway in TE cells (Fig. 2C), despite the observation that LatB treatment leads to Hippo activation and cytoplasmic localization of Yap in 3T3 cells (Fig. S1B). Similarly, neither inhibition nor induction of microtubule polymerization by nocodazole and taxol, respectively, affects Hippo signaling (Fig. 2D). The effects of CCD, LatB, nocodazole and taxol on the cytoskeleton organization in embryos are demonstrated in Fig. S1C,D. These data suggest that, unlike in cultured cells, cytoskeleton remodeling does not affect the Hippo pathway in the blastocyst. Therefore, Rho regulates Hippo signaling independently of cytoskeleton remodeling in peri-implantation embryos.

Rho is also involved in cell polarity regulation (Etienne-Manneville and Hall, 2002) and it has been shown that inhibition of Rho-ROCK signaling promotes ICM specification by impairing the apical-basal polarization and activating the Hippo pathway in the blastocyst (Kono et al., 2014). We then addressed whether Rho represses Hippo signaling through regulating cell polarity. Embryos treated with C3 for 2 and 12 h were harvested at the late morula stage and the distribution of aPKC and E-cadherin (E-cad) were examined by immunofluorescence. C3 treatment for 2 h does not alter the apical distribution of aPKC and the basal-lateral localization of E-cad in a majority of embryos, while this treatment is sufficient to activate the Hippo pathway and leads to cytoplasmic localization of Yap in TE cells. Prolonged C3 treatment (12 h) compromises the polarized distribution of aPKC and E-cad, and activates Hippo signaling in TE cells (Fig. 2E,F). These data demonstrate that disruption of cell polarity is not required for the activation of Hippo by inhibition of Rho.

Rho acts upstream of Amot and Nf2 to suppress Hippo signaling

To elucidate the mechanism by which Rho suppresses the Hippo pathway in TE cells, we then investigated the relationship of Rho and known Hippo regulators in the blastocyst: Amot and Nf2. *Nf2* siRNA or control siRNA, together with *H2B-mCherry* mRNA, were injected into one blastomere of the two-cell embryo. At the late morula stage, embryos were treated with or without C3 for 2 h. C3 treatment leads to cytoplasmic distribution of Yap in TE cells of the embryos injected with control siRNA. In contrast, progeny cells derived from the two-cell blastomere injected with *Nf2* siRNA are resistant to C3 treatment, and the nuclear localization of Yap is retained in these cells after C3 treatment (Fig. 3A). Consistently, suppression of Nf2 activity by dominant-negative Nf2 (dnNf2) also promotes nuclear distribution of Yap, and renders the nuclear localization of Yap insensitive to C3 treatment (Fig. 3B). Similarly, downregulation of *Amot* by siRNA or double-stranded RNA (dsRNA) induces C3 resistance (Fig. 3C,D), even though a smaller fraction of cells with downregulated *Amot* maintain the nuclear localization of Yap after C3 treatment when compared with cells expressing dnNf2. This might be due to incomplete knockdown of Amot and the redundancy of Amotl2. When Amot and Amotl2 are simultaneously knocked down, more cells display nuclear localization of Yap and resistance to C3 treatment, suggesting the redundancy of Amot and Amotl2 in mediating the effect of Rho on Hippo (Fig. S2C). Altogether, these data indicate that both Nf2 and Amot are essential for the activation of Hippo signaling upon inhibition of Rho.

Development (2017) 144, 3957-3967 doi:10.1242/dev.157917

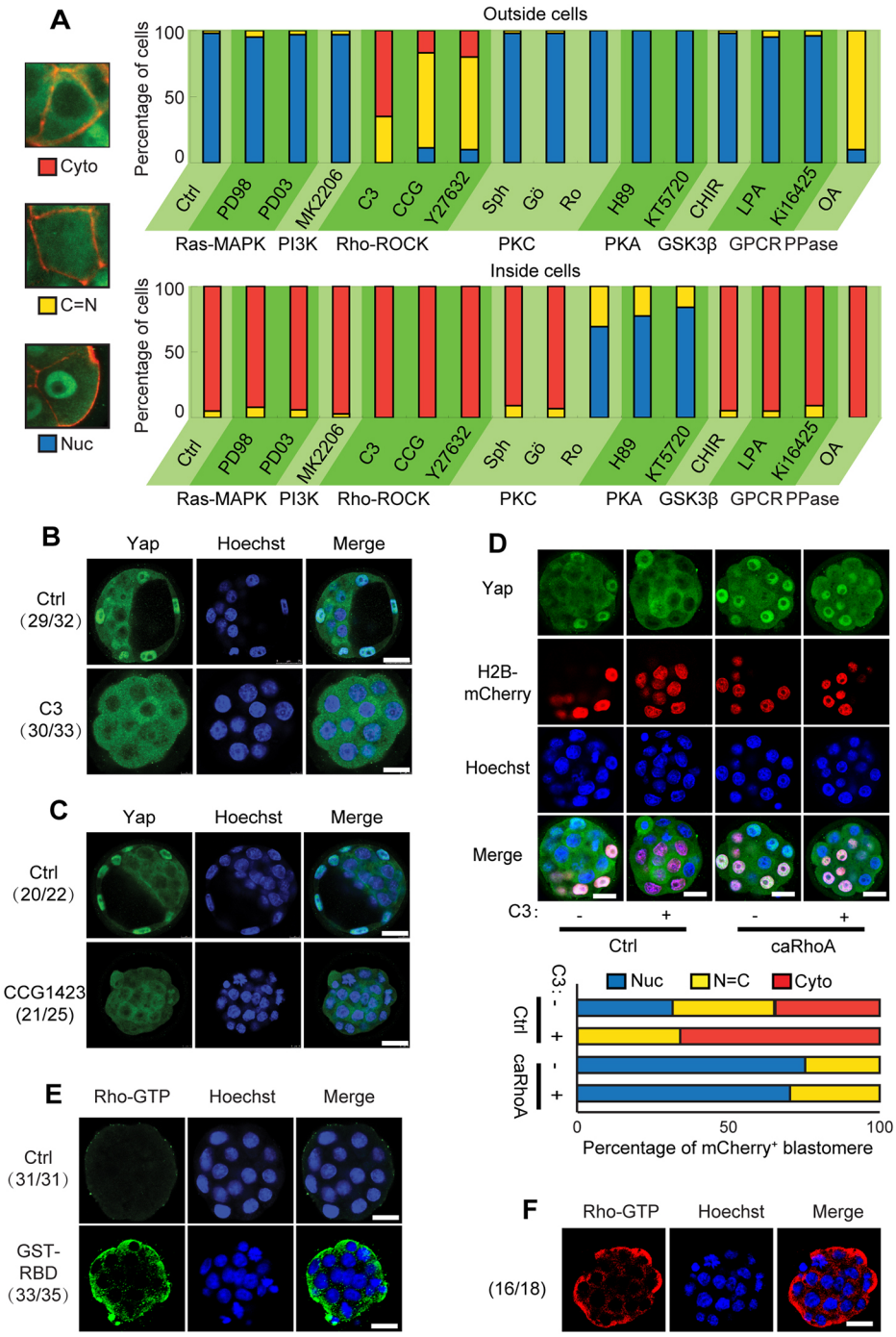

Fig. 1. Rho-ROCK signaling represses the Hippo pathway in TE cells. (A) Late morula and early blastocysts were treated with inhibitors or activators for various signaling pathways at concentrations indicated in Table S1 for 2 h. The resulting embryos were immunostained for Yap (green). F-actin was stained with phalloidin (red) to show the cell outline. The left panels are representative images of blastomeres with cytoplasmic, equal and nuclear distributions of Yap. The right panels summarize the Yap distribution in blastomeres (from >10 embryos) treated with inhibitors or activators for signaling pathways. (B,C) Inhibition of Rho activates the Hippo pathway in TE cells. Late morula and early blastocysts were treated with inhibitors of the Rho signaling pathway, C3 transferase (B) and CCG1423 (C) for 2 h and subjected to immunofluorescence. The numbers in parentheses indicate the number of embryos represented in the image from three independent experiments/the total number of embryos from three independent experiments. (D) One blastomere of the two-cell embryo was injected with *caRhoA* and *H2B-mCherry* mRNAs or *H2B-mCherry* mRNA only (Ctrl). At the late morula stage, embryos were treated with C3 for 2 h and fixed for immunofluorescence assay. mCherry fluorescent signals mark the progeny cells from the injected two-cell blastomere. The fractions of mCherry-positive blastomeres (from >10 embryos per condition) with cytoplasmic, equal and nuclear YAP distributions were summarized in the bottom panel. (E) The distribution of active GTP-bound Rho (Rho-GTP) in the blastocyst detected by Rho-GTP affinity assay. The GST-RBD protein was omitted for the control group. (F) Immunofluorescence staining of late morula/early blastocysts with an antibody (NewEast Biosciences) specifically recognizing active RhoA. Scale bars: 25 µm.

Amot binds to F-actin in TE cells

It is noteworthy that Amot is restricted to the apical domain of TE cells, whereas it is evenly distributed in the plasma membrane of ICM cells (Hirate et al., 2013; Leung and Zernicka-Goetz, 2013). Even though we have demonstrated that disruption of cell polarity is not required for Hippo activation by inhibition of Rho, it remains possible that Rho regulates the polarized distribution of Amot in TE cells. Indeed, treating embryos with ROCK inhibitor Y27632 from the two-cell stage leads to altered localization of Amot (Mihajlović and Bruce, 2016). Thus, we examined the localization of Amot in morula before and after C3 treatment, and found that Amot spreads out to the basolateral region in TE cells after 2 h of C3 treatment (Fig. 4A).

The next question we asked is to which polarized molecule in TE cells does Amot anchor? Amot is known as an F-actin-binding protein (Ernkvist et al., 2006). F-actin is apically distributed in TE cells (Liu et al., 2013). We then tested whether Amot is associated with F-actin in TE cells. First, ectopically expressed wild-type Amot colocalizes with F-actin in TE cells (Fig. 4B). Phosphorylation of S176 in Amot leads to dissociation of Amot from F-actin (Hirate et al., 2013). Replacing S176 with alanine (Amot-SA) does not change the colocalization of Amot and F-actin, whereas the mutation of S176 to an aspartate (Amot-SD), mimicking a phosphorylated residue, results in diffuse cytoplasmic distribution of Amot-SD (Fig. 4B). These data imply the association of Amot with F-actin in TE cells. To further validate this conclusion, embryos were treated

Development (2017) 144, 3957-3967 doi:10.1242/dev.157917

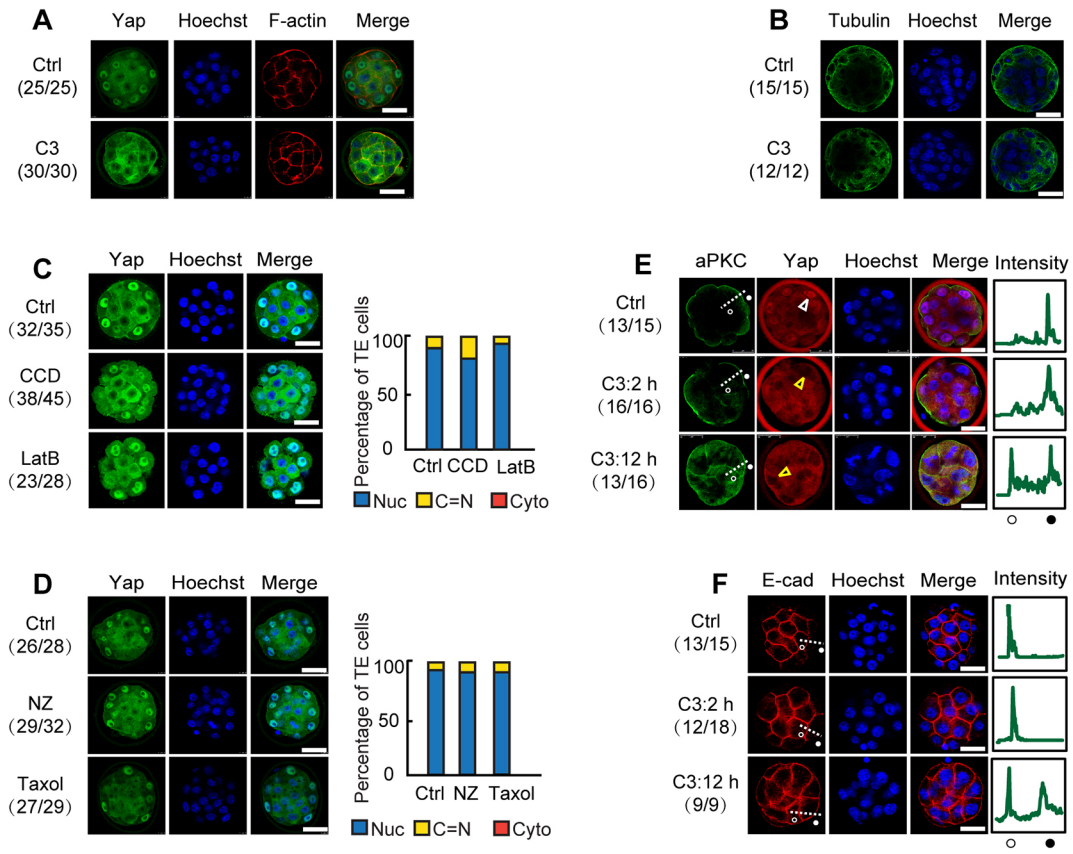

Fig. 2. The inhibitory effect of Rho on the Hippo pathway is not mediated by cytoskeleton remodeling or cell polarity. (A,B) Late morula/early blastocysts with or without C3 treatment were immunostained for F-actin, Yap (A) and tubulin (B). (C) Inhibition of actin polymerization does not affect Hippo signaling in the blastocyst. Late morula and early blastocysts were treated with actin polymerization inhibitors 1 µM CCD and 1 µg/ml LatB for 2 h, and subjected to immunofluorescence. (D) Similar to C, except that embryos were treated with chemicals affecting microtubule dynamics, 1 µM nocodazole (NZ) and 5 µM taxol. (C,D) The fractions of blastomeres (from >10 embryos per condition) with cytoplasmic, equal and nuclear YAP distributions are summarized in the right-hand panels. (E,F) Rho inhibition induces the activation of Hippo signaling before cell polarity is disrupted. Embryos were treated with C3 transferase for 2 or 12 h, and collected at the late morula/early blastocyst stage for immunofluorescence. (E) Immunofluorescence detection of aPKC. A white triangle indicates a TE cell with nuclear localized Yap; yellow triangles mark TE cells with Yap restricted to the cytoplasm. (F) Immunofluorescence detection of E-cadherin (E-cad). The right-most panels show the quantified intensity of aPKC (E) or E-cad (F) immunofluorescence signals along the dashed lines. Open circles mark the basolateral region; closed circles indicate the apical region. The numbers in parentheses indicate the number of embryos represented in the image from three independent experiments/the total number of embryos from three independent experiments. Scale bars: 25 µm.

with LatB to disrupt F-actin organization. Apical F-actin becomes fragmented. The distribution of both wild-type Amot and Amot-SA still overlaps with F-actin, suggesting Amot indeed binds to F-actin in TE cells (Fig. 4B).

Rho promotes the binding of Amot to F-actin by preventing S176 phosphorylation

To demonstrate that Rho regulates the binding of Amot to F-actin, Flag-tagged Amot, together with caRhoA or dominant-negative RhoA (dnRhoA), were expressed in MCF-7 cells. As expected, Amot-SD diffuses in the cytoplasm, not overlapping with F-actin, regardless of whether caRhoA or dnRhoA is expressed. In contrast, Amot-WT and Amot-SA colocalize with F-actin, with or without caRhoA expression. In the presence of dnRhoA, the colocalization of Amot-WT and F-actin is disrupted. However, the colocalization of Amot-SA and F-actin is resistant to dnRhoA, implying that phosphorylation of Amot S176 plays a pivot role in regulating the association between Amot and F-actin by Rho (Fig. 4C and Fig. S3B). In the blastocyst, a similar observation was made. In TE cells, inhibition of Rho by C3 leads to Amot-WT spreading out from the apical region to the basolateral region, whereas Amot-SA is restricted at the apical region and undetectable at the lateral region, even after C3 treatment (Fig. 4D). Moreover, western blot showed that caRhoA expression indeed decreases the level of phosphorylated Amot at S176 (p-Amot), and that the level of p-Amot is elevated upon dnRhoA expression in HEK293T cells (Fig. 4E). Consistently, C3 treatment of embryos also enhances the level of p-Amot (Fig. 4F). These data indicate that Rho prevents the phosphorylation of Amot S176 to stabilize the interaction between Amot and F-actin.

Nf2 recruits Amot to the plasma membrane

We have shown that Amot is anchored to apical F-actin in TE cells. Upon C3 treatment, Amot becomes phosphorylated at S176, is dissociated from F-actin and spreads out to the basolateral membrane of TE cells, consequently activating the Hippo pathway. Which protein(s) facilitate the basolateral membrane localization of Amot? How does basolaterally localized Amot activate Hippo signaling? Nf2 has been shown to be essential for the activation of Hippo signaling in the blastocyst (Cockburn et al., 2013), as well as for the activation of Hippo by Rho inhibition in TE cells (Fig. 3A,B). In addition, Nf2 activates the Hippo pathway by recruiting Lats to the plasma membrane (Yin et al., 2013). And Nf2 is evenly distributed in the plasma membrane of both TE and ICM cells (Cockburn et al., 2013). To test whether Nf2 is able to recruit

Development (2017) 144, 3957-3967 doi:10.1242/dev.157917

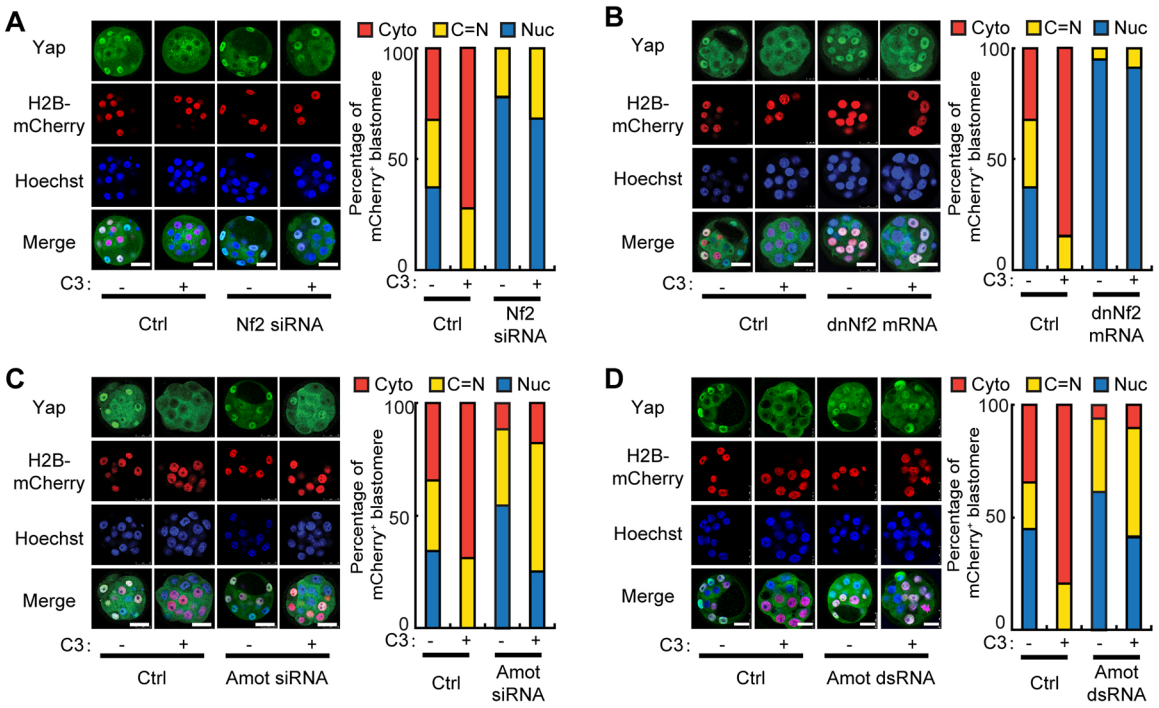

Fig. 3. Both Nf2 and Amot are required for the activation of Hippo signaling in TE cells induced by Rho inhibition. (A) One blastomere of the two-cell embryo was injected with *Nf2* siRNA or negative control siRNA (Ctrl), together with *H2B-mCherry* mRNA. At the late morula stage, embryos were treated with C3 for 2 h, and fixed for immunofluorescence assay. mCherry fluorescent signals mark the progeny cells from the injected two-cell blastomere. Left panels show the representative images. Right panel summarizes the data from at least 20 embryos and more than 100 mCherry-positive blastomeres. (B-D) Similar to A, except that *dnNf2* mRNA (B), Amot siRNA (C) and Amot dsRNA (D), together with *H2B-mCherry* mRNA, were injected into one blastomere of the two-cell embryo. Scale bars: 25 µm. Knockdown efficiencies of *Nf2* siRNA, *Amot* siRNA and dsRNA are shown in Fig. S2.

Amot to the plasma membrane, Amot-GFP, with or without Nf2-mCherry, was expressed in HEK293T cells. In the absence of Nf2-mCherry, Amot-GFP is located in the cytoplasm, likely associated with F-actin. When Nf2-mCherry is expressed, Amot-GFP colocalizes with Nf2-mCherry at the plasma membrane (Fig. 5A). Experiments repeated in HeLa cells (Fig. S4A) also support the conclusion that Nf2 recruits Amot to the plasma membrane. Moreover, knockdown of *Nf2* disrupts the membrane localization of Amot in ICM cells. In contrast, Amot distribution at the apical region of TE cells is maintained upon *Nf2* knockdown (Fig. 5B). These data suggest that Amot is recruited to the membrane by Nf2 in ICM cells, whereas the apical distribution of Amot in TE cells depends on the interaction between Amot and F-actin.

It has been shown that Amot interacts with Nf2 (Hirate et al., 2013; Yi et al., 2011; Li et al., 2015). With co-immunoprecipitation, we also detected the interaction between Amot and Nf2, which is regulated by Rho activity. caRhoA attenuates the association of Amot and Nf2, whereas dnRhoA slightly enhances the interaction between Amot and Nf2 (Fig. 5C). More importantly, Amot and Nf2 collaboratively activate the Hippo pathway, elevating the level of p-Lats1/2 and p-Yap (Fig. 5D). In addition, caRhoA blocks the plasma membrane recruitment of Amot by Nf2 (Fig. 5E), suggesting that Rho might regulate the Hippo pathway through repressing the interaction between Amot and Nf2.

Phosphorylation of Amot S176 and the binding of RhoA to Amot CC domain regulate the interaction between Amot and Nf2

Given the important role of Amot S176 phosphorylation in regulating the interaction between Amot and F-actin, we suspected that phosphorylation of Amot S176 may affect the association of Amot and Nf2. To test this hypothesis, Amot-WT, SD and SA were co-expressed with Nf2 in HEK293T cells. Nf2 is able to recruit Amot-WT and Amot-SD, but not Amot-SA to the plasma membrane (Fig. S4B), suggesting that Amot has to be phosphorylated to allow its interaction with Nf2. We then asked whether Rho attenuates the interaction between Amot and Nf2 through blocking the phosphorylation of Amot S176. Expression of caRhoA impairs the recruitment of both Amot-WT and Amot-SD to the plasma membrane by Nf2 (Fig. 5E), whereas the plasma membrane localization of Nf2 is not affected by caRhoA (Fig. S4C), implying that Rho may suppress the interaction between Amot and Nf2 independently of Amot S176 phosphorylation. Nevertheless, compared with Amot-WT, Amot-SD is more resistant to caRhoA-induced dissociation from the plasma membrane. Upon caRhoA overexpression, ~45% cells retain the plasma membrane distribution of Amot-SD, whereas the plasma membrane distribution of Amot-WT persists in only a few cells (~10%) (Fig. 5E). These data suggest that dephosphorylation of Amot S176 contributes to the attenuated interaction between Amot and Nf2 by Rho. Moreover, co-immunoprecipitation experiments showed that caRhoA is able to weaken the association of Nf2 with Amot, regardless of the phosphorylation status of Amot S176 (Fig. 5F). The Nf2-interacting site on Amot has been mapped to the CC domain (Li et al., 2015). The binding between Nf2 and the CC domain of Amot is also reduced by caRhoA, even though the N-terminal domain of Amot, including S176, is absent (Fig. 5G). These data suggest that additional mechanism(s), other than regulating Amot S176 phosphorylation, are employed by Rho to suppress the binding between Amot and Nf2.

We hypothesized that Rho might compete with Nf2 in binding to Amot. With co-immunoprecipitation experiments, the interaction between caRhoA and Amot was detected (Fig. 5H). We further

Development (2017) 144, 3957-3967 doi:10.1242/dev.157917

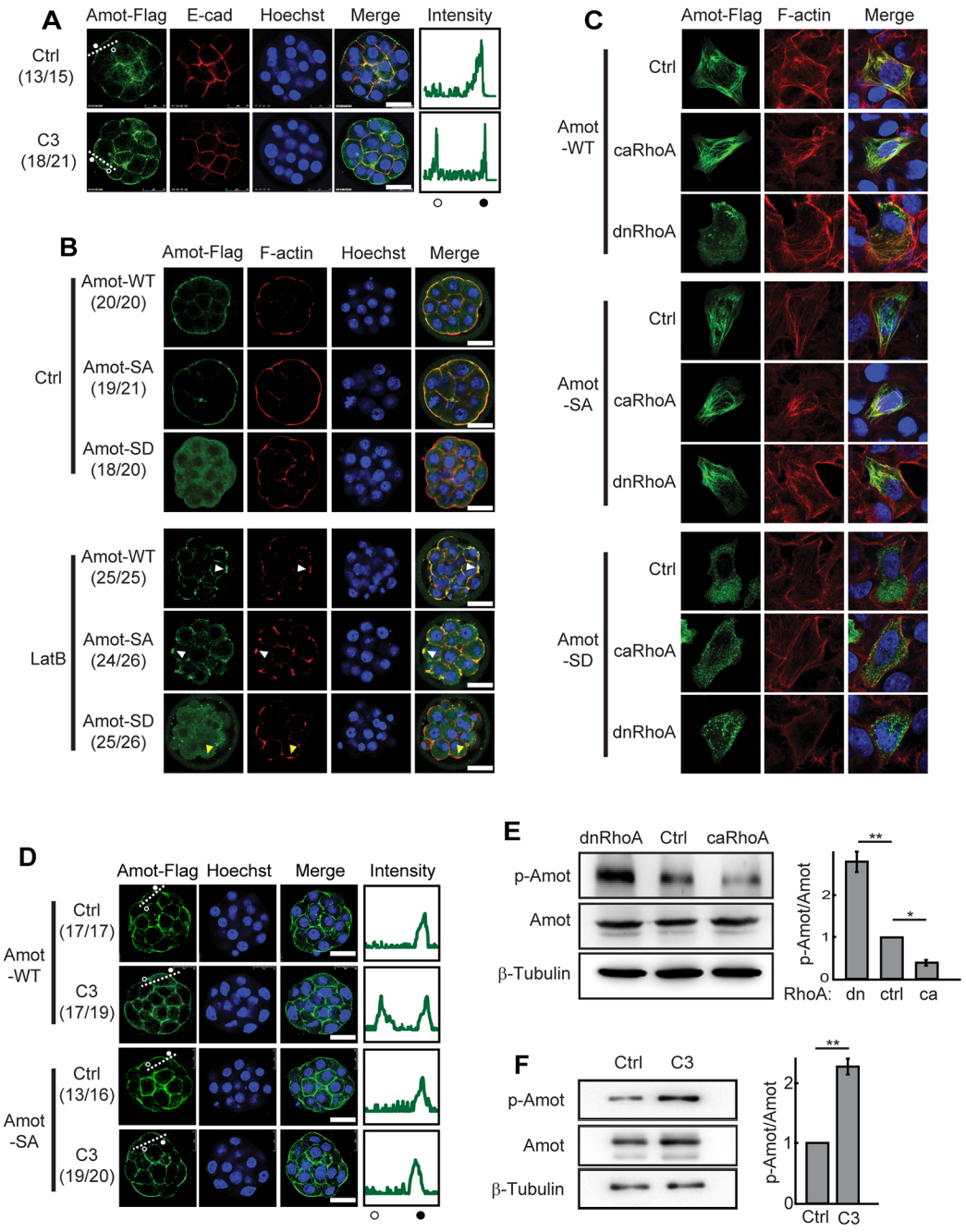

Fig. 4. Rho regulates the distribution and the phosphorylation of Amot. (A) *Amot-Flag* mRNA was injected into zygotes. Late morula and early blastocysts were treated with C3 transferase for 2 h and subjected to immunofluorescence with Flag antibody. The right-most panels show the quantified intensity of Amot-Flag immunofluorescence signals along the dashed lines. Open circles mark the lateral region; filled circles indicate the apical region. E-cadherin is included to show the basolateral region. (B) mRNAs encoding Flag-tagged Amot-WT, SA and SD were injected into zygotes. Late morula and early blastocysts were treated with LatB for 2 h and subjected to immunofluorescence with Flag antibody. F-actin was stained with phalloidin. White arrowheads indicate the colocalization of Amot and F-actin in LatB-treated embryos; yellow arrowheads indicate F-actin without enriched Amot-SD signaling. (C) Plasmids expressing Flag-tagged Amot-WT, SA or SD, together with control empty vector and expression vectors for caRhoA or dnRhoA were co-transfected into MCF-7 cells. Twenty-four hours after transfection, cells were immunostained with Flag antibody, and F-actin was stained with phalloidin. The F-actin signal is weak in cells expressing dnRhoA. To show the overlap between Amot and F-actin, the F-actin signals in cells expressing dnRhoA, as well as Amot-WT or SA, are adjusted to match the intensity in cells without dnRhoA. The percentages of cells with colocalized Amot and F-actin were quantified and are shown in Fig. S3. (D) mRNAs encoding Flag-tagged Amot-WT and SA were injected into zygotes. Late morula and early blastocysts were treated with C3 transferase for 2 h, and subjected to immunofluorescence with Flag antibody. The right-most panels show the quantified intensity of Amot-Flag immunofluorescence signals along the dashed lines. Open circles mark the lateral region; filled circles indicate the apical region. Scale bars: 25 µm. (E) Control empty vector and expression vectors for caRhoA and dnRhoA were transfected into HEK293T cells. Twenty-four hours after transfection, cells were harvested for western blot. (F) Late morula and early blastocysts were treated with or without C3 transferase for 2 h, and embryos were harvested for western blot. The band intensities of Amot and p-Amot were quantified, and the ratios of p-Amot to Amot were plotted. Data are shown as mean±s.d. (n=3). $^{**}P$<0.01, $^{*}P$<0.05. The numbers in parentheses indicate the number of embryos represented in the image from three independent experiments/the total number of embryos from three independent experiments.

Development (2017) 144, 3957-3967 doi:10.1242/dev.157917

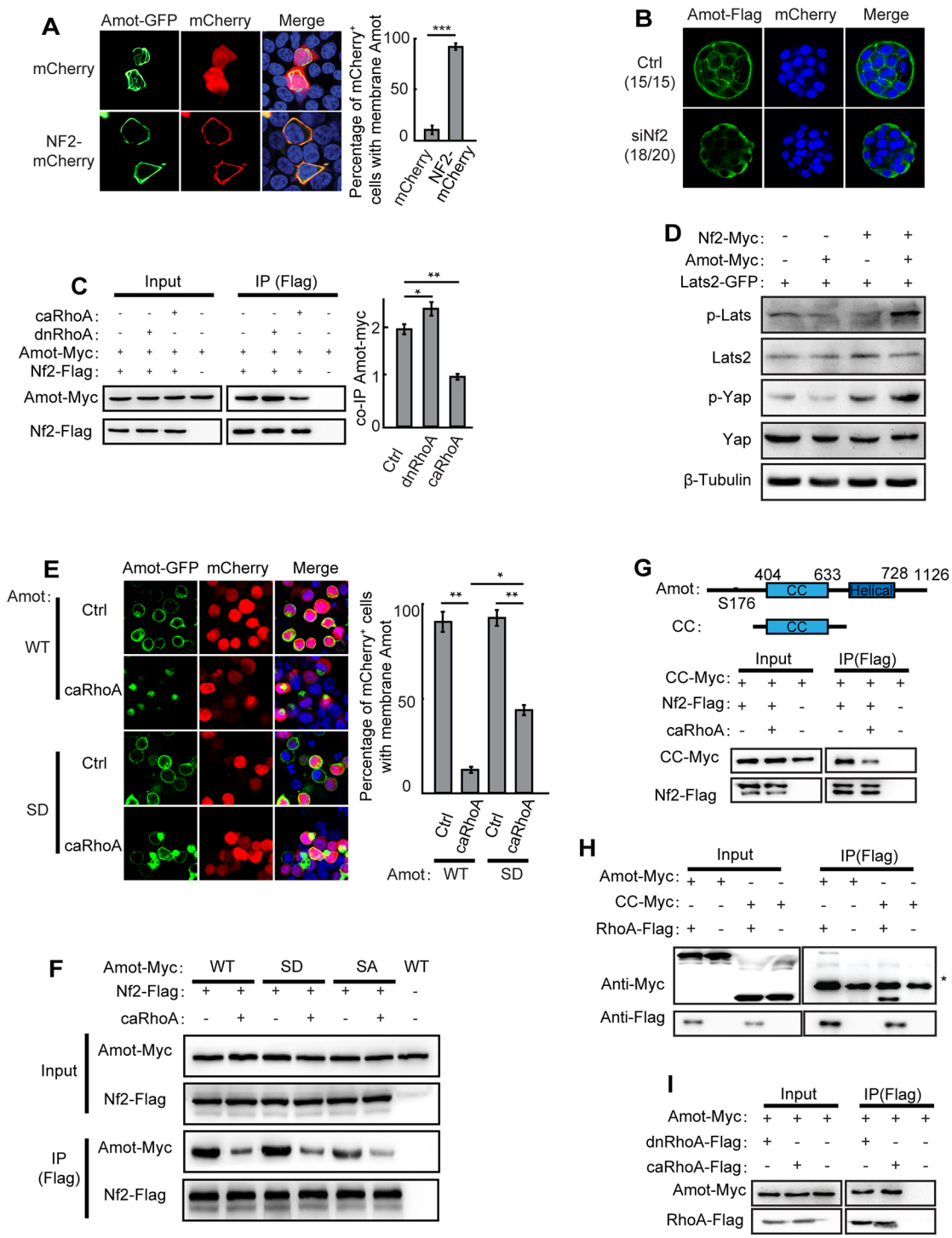

Fig. 5. See next page for legend.

demonstrated that caRhoA also interacts with the CC domain of Amot, which also mediates the interaction with Nf2 (Fig. 5H). Conversely, Nf2 overexpression also reduces the interaction between caRhoA and Amot (Fig. S4D). Thus, competitive binding at the CC domain of Amot allows RhoA to suppress the interaction between Nf2 and Amot. Both caRhoA and dnRhoA binds to Amot, and the binding between caRhoA and Amot is slightly stronger than that of dnRhoA and Amot (Fig. 5I), implying that Rho activity is not essential for the binding between RhoA and Amot.

Another possible mechanism by which Rho could reduce the association of Nf2 and Amot is post-translational modifications (PTMs) of these proteins. The Amot CC domain was expressed without or with caRhoA. The resulting protein lysates were resolved in regular SDS-PAGE and Phos-tag gels. No difference in the electrophoretic mobility of Amot CC domain was detected in either gels (Fig. S4E,F), implying that caRhoA might not alter the PTM status of the CC domain. Nevertheless, some PTMs do not change the gel mobility of proteins. Therefore, we cannot rule out the

Development (2017) 144, 3957-3967 doi:10.1242/dev.157917

Fig. 5. Rho regulates the interaction between Nf2 and Amot. (A) Amot-GFP expression plasmid, together with plasmids expressing mCherry or Nf2-mCherry, was transfected into HEK293T cells. Twenty-four hours after transfection, confocal images were taken. The percentages of mCherry-positive cells with Amot localized to the cytoplasmic membrane were quantified and plotted (>100 mCherry-positive cells for each condition, three independent repeats). Data are shown as mean±s.d. (n=3), ***P<0.001. (B) Zygotes were injected with control or *Nf2* siRNA, together with *Amot-Flag* mRNA. At late morula stage, embryos were stained with Flag antibody. (C) Plasmids expressing Amot-Myc and Nf2-Flag, with or without dnRhoA or caRhoA expression plasmid, were co-transfected into HEK293T cells. Twenty-four hours after transfection, cells were harvested and subjected to co-immunoprecipitation with anti-Flag M2 beads. Quantification results of the Amot-Myc signals normalized to the Nf2-Flag are shown in the right-hand panel. **P<0.01, *P<0.05. (D) HEK293T cells were transfected with control empty expression plasmid and plasmids expressing Amot-Myc and Nf2-Myc separately or together. Cells were harvested for western blot 24 h after transfection. (E) Similar to A, except that Amot-GFP (WT or SD) and Nf2 expression plasmids, together with plasmids expressing mCherry or caRhoA-IRES-mCherry, were transfected into HEK293T cells. **P<0.01, *P<0.05. (F) Similar to C, except that plasmids expressing Amot-Myc (WT, SA and SD) and Nf2-Flag, with or without caRhoA expression plasmid, were co-transfected into HEK293T cells. (G) Similar to C, except that plasmids expressing Nf2-Flag and Myc-tagged CC domain of Amot (CC-Myc), with or without caRhoA expression plasmid, were co-transfected into HEK293T cells. (H) Plasmids expressing Amot-Myc or CC-Myc, with or without caRhoA-Flag expression plasmid, were transfected into HEK293T cells. Twenty-four hours after transfection, cell lysates were prepared for co-immunoprecipitation with anti-Flag M2 beads. The IgG band in the immunoprecipitation blot is marked with an asterisk. (I) HEK293T cells were transfected with plasmids expressing caRhoA-Flag or dnRhoA-Flag, together with Amot-Myc expression plasmid. The co-immunoprecipitation experiment was performed 24 h after transfection. The numbers in parentheses indicate the number of embryos represented in the image from three independent experiments/the total number of embryos from three independent experiments.

possibility that Rho regulates the binding of Amot to Nf2 through PTMs.

So far, we have characterized two mechanisms by which Rho can prevent the binding of Amot and Nf2 (Fig. 6A). First, active Rho blocks the phosphorylation of Amot S176, thus stabilizing the association between unphosphorylated Amot and F-actin, and reducing the concentration of free Amot. Second, active Rho competes with Nf2 in binding to the CC domain of Amot. The second mechanism might be complementary to the first one in suppressing the interaction between Nf2 and Amot transiently dissociated from F-actin. The cooperation of these two mechanisms might be crucial for the suppression of the Hippo pathway in TE cells, in which Amot and Nf2 are colocalized in the apical region.

DISCUSSION

In this study, we have identified Rho as a negative regulator of the Hippo pathway in TE cells, and have demonstrated that Rho suppresses the Hippo pathway through modulating the interaction between Amot and Nf2. In TE cells of the blastocyst, Rho is active. Amot is unphosphorylated and binds to apical F-actin. Moreover, Rho occupies the CC domain of Amot, and prevents the binding between Nf2 and Amot that is transiently dissociated from apical F-actin. Without the formation of Amot and the Nf2 complex, Lats1/2 cannot be activated. Thus, the Hippo pathway is inactive, and Yap translocates into the nucleus to promote TE differentiation. In contrast, the activity of Rho is absent in ICM cells. Amot becomes phosphorylated and dissociated from F-actin, which allows the interaction between Nf2 and Amot. A complex formed with Amot and Nf2, as well as with other proteins, leads to the activation of Hippo signaling and cytoplasmic retention of Yap, allowing the specification of ICM cell fate (Fig. 6B).

What features of the blastocyst lead to the differential status of Rho in TE and ICM cells? Previous results and our data support that cell contacts are essential for the differential regulation of Rho in the blastocyst. First, when cell contacts are impaired in embryos lacking both maternal and zygotic E-cadherin, nuclear Yap localization and Cdx2 expression in TE cells are not affected. Rather, more Cdx2 positive cells are present in E-Cadherin knockout embryos (Stephenson et al., 2010). Second, when blastomeres of the 32-cell embryo are dissociated into single cells, the Hippo pathway is repressed and Yap becomes localized to the nucleus, regardless of the original inside or outside positions of the cells (Hirate et al., 2013). Moreover, when dissociated blastomeres were treated with C3 to inhibit Rho, Yap is distributed in the cytoplasm in all cells (Fig. S1E). These data imply that cell contacts inactivate Rho, and subsequently activate the Hippo pathway in ICM cells. It has been suggested that cell polarity of TE cells is required for inactivating the Hippo pathway, and that difference in cell contractility between polar and apolar cells regulates the Hippo pathway and cell fate (Hirate et al., 2013; Cao et al., 2015; Anani et al., 2014; Maître et al., 2016). Moreover, isolated eight-cell blastomeres become polarized, and the apical domain is required and sufficient for the specification of TE cell fate (Korotkevich et al., 2017). Cell contacts, cell polarity and cell contractility are tightly co-regulated. It is very likely that cell contacts might regulate Rho through affecting cell polarity and cell contractility in the blastocyst. Cell contacts inhibit cell polarity in ICM cells by preventing the formation of polarized apical domain, resulting in high cell contractility. In contrast, cell contacts stabilize the cell polarity of TE cells by separating the apical and basolateral regions, thus maintaining low cell contractility. When cell contacts are disrupted either by E-Cadherin knockout or blastomere dissociation, inside cells might initiate the formation of apical domain and reduce contractility, whereas the polarity of outside cells is compromised, but still maintained. The polarity and low contractility of cells consequently leads to Rho activation, Hippo suppression and nuclear localization of Yap.

GPCR signaling has been shown to regulate the Hippo pathway through Rho GTPases (Yu et al., 2012, 2013). Our data rule out the possibility that Rho is activated by GPCRs coupled to $G\alpha_{12/13}$ or $G\alpha_{q/11}$ in the TE. Neither the ligand for GPCRs coupled to $G\alpha_{12/13}$ or $G\alpha_{q/11}$, lysophosphatidic acid (LPA), nor the LPA antagonist Ki16425 alters Hippo signaling in the blastocyst (Fig. 1A). PKA, which mediates the signaling from $G\alpha_s$-coupled GPCRs to suppress Rho and subsequently activate Hippo signaling in breast cancer cells (Yu et al., 2013), was identified as an activator for the Hippo pathway in ICM cells in our initial screen. It raises the possibility that $G\alpha_s$-coupled GPCRs activate PKA, which in turn suppresses Rho in the ICM. However, when embryos were treated with PKA inhibitor H89 and Rho inhibitor C3 simultaneously, the Hippo pathway is inactivated and Yap becomes nuclear localized in all blastomeres, regardless of their position in the embryo (Fig. S1F). The data indicate that Rho is not downstream of PKA or $G\alpha_s$-coupled GPCRs in regulating the Hippo pathway in the blastocyst. The relationship between PKA and Rho in modulating Hippo signaling in the blastocyst needs further investigation.

It has been shown that Rho GTPases repress the Hippo pathway through promoting F-actin formation in cultured cells (Zhao et al., 2012; Mo et al., 2012; Yu et al., 2012; Feng et al., 2014). However, in TE cells, cytoskeleton remodeling is uncoupled from the Hippo pathway in the blastocyst. Drugs affecting cytoskeleton dynamics, including CCD, LatB, nocodazole and taxol, do not affect Hippo signaling in the blastocyst (Fig. 2C,D). It is very likely that F-actin and microtubule lose their mechanosensor function in the

Development (2017) 144, 3957-3967 doi:10.1242/dev.157917

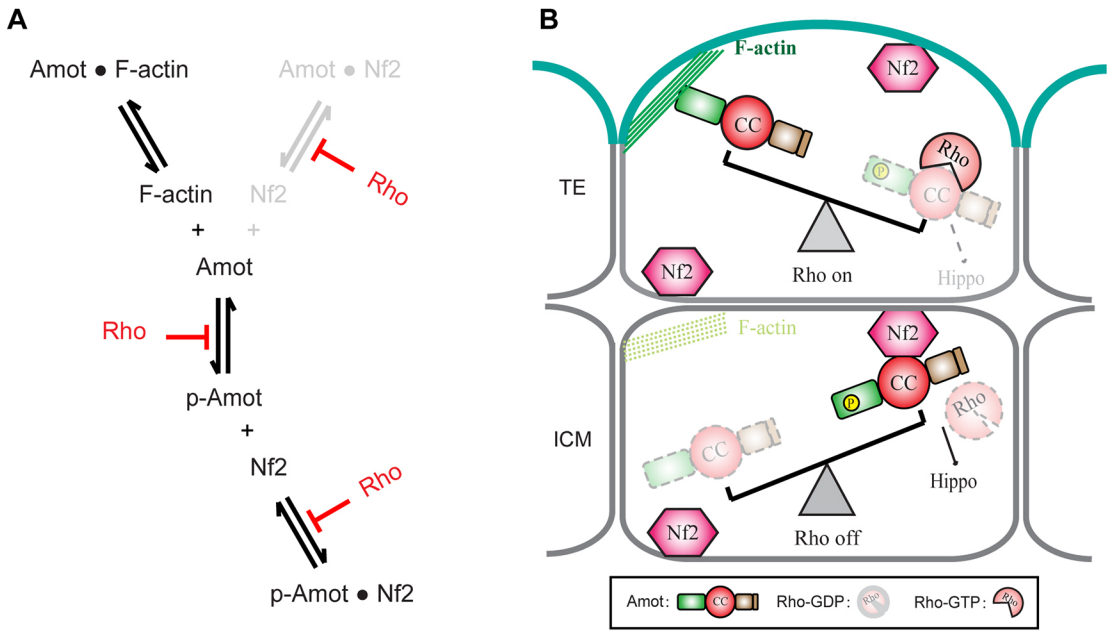

Fig. 6. A working model to explain how Rho differentially regulates the Hippo pathway in the blastocyst. (A) Two mechanisms by which Rho can prevent the interaction between Amot and Nf2. Active Rho blocks the phosphorylation of Amot S176, facilitating the binding of Amot to F-actin. In addition, active Rho binds to the CC domain of Amot to prevent the binding between Amot and Nf2. The binding between unphosphorylated Amot and Nf2 is shown in gray to indicate that it is a weak interaction, compared with the interaction between Amot and F-actin. (B) In TE cells, Rho is active and blocks the phosphorylation of Amot S176 (green). Unphosphorylated Amot interacts with F-actin through its N-terminal domain. Active Rho binds to the CC domain of Amot. These interactions prevent the association between Amot and Nf2, thus failing to activate the Hippo pathway. In ICM cells, less F-actin exists in the absence of active Rho. In addition, Amot S176 becomes phosphorylated. Consequently, Amot is released from F-actin and interacts with Nf2 to activate the Hippo pathway. Unphosphorylated Amot in ICMs and p-Amot in TE cells are shown in dotted gray outlines to indicate their low abundance in corresponding cells.

blastocyst. In support of this, both F-actin and microtubule are enriched at the apical region of the blastocyst, a distinct distribution pattern compared with that in cultured cells. Nevertheless, F-actin is still involved in regulating the Hippo pathway in the blastocyst, through sequestering Amot. Inhibitors of actin polymerization, such as CCD and LatB, disrupt the integrity of F-actin network, but do not interfere with the binding of Amot to the fragmented F-actin. Therefore, neither CCD nor LatB perturbs the Hippo pathway in the blastocyst. Only Rho inhibition by C3, which induces the dissociation of Amot from F-actin, leads to the activation of Hippo signaling in TE cells.

Regulating the phosphorylation status of Amot S176 by Rho signaling is a crucial step in modulating the interaction between Amot and F-actin, and activating the Hippo pathway. Yet how Rho prevents the phosphorylation of Amot S176 is unknown. Lats kinases have been shown to phosphorylate Amot S176 (Hirate et al., 2013). However, our data showed that upon Amot knockdown by siRNA or dsRNA, the Hippo pathway is not activated in TE cells after C3 treatment, suggesting that Amot is upstream of Lats kinases, and downstream of Rho. It seems that Amot is phosphorylated by a kinase other than Lats in TE cells upon Rho inhibition. Yet it remains possible that Amot and Nf2 collaboratively activate Lats kinases, and activated Lats kinases phosphorylate Amot. This positive feedback circuit formed by Amot/Nf2 and Lats may be essential for quick and efficient activation of the Hippo pathway. Disruption of any component in the circuit leads to a failure in full activation of the Hippo pathway.

In TE cells, Amot is restricted to the apical region by binding to F-actin (Fig. 4A). How does Amot anchor to the plasma membrane in ICM cells and C3-treated TE cells? We have shown that, in HEK293T and HeLa cells, Nf2 recruits Amot to the plasma membrane (Fig. 5A and Fig. S4A). Amot dissociates from the membrane of ICM cells upon *Nf2* knockdown (Fig. 5B), further confirming that Amot is recruited to the basolateral membrane by Nf2. In addition, other components of adherens junction might contribute to the membrane distribution of Amot in the blastocyst. The interaction between E-cadherin and Amot has been demonstrated by co-immunoprecipitation experiments (Hirate et al., 2013).

Taken together, our results demonstrated the crucial role of Rho in the differential regulation of the Hippo pathway in the TE and the ICM. In contrast to the prevailing view that Rho represses Hippo signaling by modulating the actin cytoskeleton, Rho inhibits the interaction between Amot and Nf2 to inactivate the Hippo pathway in TE cells. These two mechanisms are not exclusive, and might cooperate to suppress the Hippo pathway in other biological systems.

MATERIALS AND METHODS

Embryo culture

All animal experiments were carried out in strict accordance with the recommendations in the Guide for the Care and Use of Laboratory Animals of the National Institutes of Health (China). The use of mice for this research is approved by Nankai Animal Care and Use Committee.

Embryo manipulation experiments were carried out as described previously (Liu et al., 2013). Female ICR mice (4-6 weeks) were induced to superovulate by intraperitoneal injections of 5 IU of pregnant mare serum gonadotropin (PMSG, Calbiochem) and, 48 h later, 5 IU human chorionic gonadotropin (hCG, Sigma). Females were then paired with ICR males overnight and checked for vaginal plugs next morning. Zygotes were flushed out from oviducts at 12 h post-hCG, and two-cell embryos were flushed out at 42-48 h post-hCG. Embryos were cultured in groups of 20-30 in a 50 µl droplet of potassium simplex optimization medium (KSOM) with amino acids (Millipore) covered by mineral oil (Sigma) in a 37°C incubator with 6.5% CO_2. The concentrations of inhibitors or activators to treat late morula and early blastocysts are listed in Table S1. All experiments were performed with groups of more than 10 embryos and repeated three times.

Development (2017) 144, 3957-3967 doi:10.1242/dev.157917

Embryo injection

For the injection of two-cell embryos, 10 mM siRNA, 100 ng/µl *Amot* dsRNA, 10 ng/µl *caRhoA* mRNA or 100 ng/µl *dnNf2* mRNA, together with 100 ng/µl H2B-mCherry mRNA, were injected into one blastomere of the late two-cell stage embryo. For control embryos, 200 ng/µl H2B-mCherry mRNA was injected into one blastomere of the late two-cell stage embryo. For zygotic injection, 200 ng/µl *Amot-Flag* (WT, SA or SD) mRNA was injected into the cytoplasm of fertilized eggs in M2 medium. We demonstrated that Yap distribution in embryos is not affected when 200 ng/µl *Amot-Flag* mRNA is injected (Fig. S3A). After injection, embryos were cultured in KSOM medium until the late morula stage.

Cell culture and transfection

HEK293T, HeLa and MCF-7 cells were cultured in DMEM (Invitrogen) supplemented with 10% fetal bovine serum, penicillin (100 U/ml) and streptomycin (100 mg/ml) under an atmosphere of 5% CO_2 at 37°C. Transfection of plasmid DNA was performed with lipofectamine 3000 (Invitrogen) according to the manufacturer's instructions. HEK293T and HeLa cells were obtained from George Daley's laboratory at Harvard Medical School (Boston, MA, USA). MCF-7 cells were purchased from ATCC. These cell lines were recently authenticated using Short Tandem Repeat DNA profiling analysis.

Immunofluorescence

Embryos were fixed in 4% paraformaldehyde for 20 min, and then permeabilized with 0.2% Triton X-100 for 30 min. After being blocked with 5% goat serum for 2 h, embryos were incubated with primary antibodies for 4-6 h at room temperature or overnight at 4°C. Embryos were then washed and incubated with secondary antibodies and/or rhodamine-phalloidin (Molecular Probes). Alexa Fluor 488 anti-mouse, Alexa Fluor 488 anti-rabbit and Alexa Fluor 594 anti-rabbit were used as secondary antibodies (Molecular Probes), and Hoechst 33342 (Sigma) was used for nuclei staining. Epifluorescent images were taken using Olympus IX81 microscope. Confocal images were captured using Leica TCS SP5 confocal microscope.

In some experiments, localization of aPKC, E-cadherin and Amot proteins along the apical-basal or apical-lateral cell polarity was assessed with the ImageJ software. After conversion to TIFF format, images were opened in ImageJ, a line was drawn across the apical and basal/lateral sides of an outer cell, and pixel intensities along this line were examined using the Plot Profile Tool.

Rho-GTP affinity assay

Analysis of active Rho protein was conducted as previously described (Berdeaux et al., 2004). Briefly, embryos were fixed with freshly prepared 4% paraformaldehyde in PBS for 30 min at room temperature. After washing, embryos were permeabilized in PBS containing 3% BSA, 0.1 M glycine and 0.05% Triton X-100, blocked in the same buffer containing 5% goat serum, and then incubated with 50 µg/ml GST-tagged Rhotekin-Rho-binding domain (GST-RBD) (RT01A, Cytoskelton) for 12 h at 4°C. Anti-GST primary antibody and Alexa Fluor 488-conjugated anti-rabbit antibody were used to visualize the GST-RBD and Rho-GTP complex. Confocal images were captured using Leica TCS SP5 confocal microscope. The specificity of Rho-GTP affinity assay is demonstrated by a negative control (C3 treated embryos) and a positive control (caRhoA-overexpressing embryos) (Fig. S1A).

siRNA, dsRNA and mRNA preparation

Amot- and *Nf2*-coding regions were amplified from cDNA of V6.5 mouse embryonic stem cells (ESCs), and inserted into the RN3P vector (a gift from Dr Na Jie). Amot was fused with 3×Flag. dnNf2 was constructed by replacing alanine for a seven amino acid stretch in the FERM domain (Johnson et al., 2002). Using *Sfi*I-cut RN3P-Amot-Flag or RN3P-dnNf2 plasmids as DNA templates, mRNA was synthesized using the mMESSAGE mMACHINE T7 transcription Kit (Life Technologies).

dsRNA was prepared as previously described (Leung and Zernicka-Goetz, 2013). The DNA template for *in vitro* transcription of *Amot* dsRNA was amplified from V6.5 mouse ESC cDNA, with the following primers, 5′-TAATACGACTCACTATAGGGTGTGTTTGGGGAGAAAAGGA-3′ and 5′-TAATACGACTCACTATAGGGAAGTCCAGGAAAAGGCCTGA-3′. *Amot* dsRNA was synthesized with the DNA template using the T7 mMESSAGE mMACHINE Kit. The dsRNA was annealed by heating to 70°C for 5 min and cooling at room temperature for 2 h. The resulting RNA sample was treated with RNase A and Proteinase K to remove ssRNA and proteins.

siRNAs were synthesized by GenePharma Corporation (Shanghai, China). *Amot* siRNA, 5′-CAGGAGAAGCCUACUCAGCUA-3′; *Nf2* siRNA, 5′-GGUGUUGGAUCAUGAUGUUTT-3′; negative control siRNA, 5′-UUCUCCGAACGUGUCACGU-3′. Stealth RNAi siRNA for *Amotl2* (Amotl2 MSS226047) was purchased from Thermo Fisher. The knockdown efficiency of *Amotl2* siRNA has been demonstrated previously (Hirate et al., 2013).

Immunoprecipitation

Expression plasmids were transfected into HEK293T cells. One day after transfection, cells were harvested and cell extracts were prepared in lysis buffer [20 mM Tris-HCl (pH 8.0), 137 mM NaCl, 10% glycerol, 1% NP-40, and 2 mM EDTA] with protease inhibitor (Roche) on ice for 30 min. After centrifugation at 12,000 ***g*** for 20 min, the supernatant was collected and incubated with anti-Flag M2 magnetic beads (Sigma) at 4°C overnight. The beads were washed three times with lysis buffer, and the bound proteins were released from the beads by boiling the beads in 2× SDS loading buffer for 5 min. Western blot was performed to detect the proteins present in immunoprecipitate samples.

Western blot

Cells were lysed and total protein concentration was measured using a BCA Protein Assay Kit (Beyotime) to ensure equal loading. Samples were resolved by SDS-PAGE followed by transferring onto a PVDF membrane (Millipore). Membranes were probed with primary antibodies. Bound primary antibodies were recognized by HRP-linked secondary antibodies (GE Healthcare). HRP activity was detected by ECL Plus (Beyotime). Digital images were taken by the automatic chemiluminescence imaging analysis system (Tanon).

RNA isolation and quantitative RT-PCR

Trizol reagent (Roche) was used for RNA purification from cultured cells. cDNA was reverse transcribed using the Transcriptor First-Strand cDNA Synthesis Kit (Roche) with random primers according to the manufacturer's instruction. Real-time PCR was carried out with FastStart Universal SYBR Green Master (Roche) in a Bio-Rad IQ5 system. mRNA relative abundance was calculated by normalizing to β-actin mRNA. The following primers were used for real-time PCR: β-actin, 5′-CAGAAGGAGATTACTGCTCT-GGCT-3′ and 5′-CAGAAGGAGATTACTGCTCTGGCT-3′; Nf2, 5′-CTC-TTGGCGTCATATGCTGT-3′ and 5′-GAGCAATTCCTCTTGGGCTA-3′; Amot, 5′-GATGTGCAACCCAGATAAGCC-3′ and 5′-TCTCTGCATCA-GGCTCTTGC-3′.

Antibodies

Primary antibodies used in this study were YAP [Santa Cruz, SC-101199; 1:1000 for western blot (WB), 1:200 for immunofluorescence (IF)], aPKC (Santa Cruz, SC-216; 1:200 for IF), E-cadherin (Abcam, ab15148; 1:200 for IF), pYAP (CST, 4911; 1:1000 for WB), LATS2 (Abcam, ab84158; 1:1000 for WB), pLATS1/2 (CST, 8654; 1:1000 for WB), Amot (Santa Cruz, sc-82491; 1:1000 for WB), pAmot (Millipore, ABS1045; 1:1000 for WB), Myc (Santa Cruz, SC-40; 1:5000 for WB), Flag (Sigma, F1804; 1:5000 for WB, 1:200 for IF), GST (Abcam, ab19256; 1:200 for IF), active RhoA-GTP (NewEast Biosciences, 26904; 1:100 for IF) and β-Tubulin (Huada, AbM59005-37B-PU; 1:10,000 for WB, 1:1000 for IF).

Statistical analysis

All data were analyzed using Student's *t*-test. Statistically significant *P* values are indicated in figures as follows: ***$P<0.001$, **$P<0.01$, *$P<0.05$.

Acknowledgements

We thank Professor Shian Wu for his critical reading of the manuscript, and the core facility at the College of Life Sciences, Nankai University, Tianjin, China.

Competing interests
The authors declare no competing or financial interests.

Author contributions
Conceptualization: L.C.; Methodology: L.W.; Investigation: X.S., Z.Y., B.L., C.L., X.R., W.Z.; Writing - original draft: X.S., L.C.; Writing - review & editing: L.C.; Visualization: X.S.; Supervision: L.C.; Project administration: L.C.; Funding acquisition: L.C.

Funding
This work was supported by the National Natural Science Foundation of China (31671497, 31622038, 31271547 and 31470081), the 111 Project Grant (B08011) and the PhD Candidate Research Innovation Fund of Nankai University (Tianjin, China).

Supplementary information
Supplementary information available online at
http://dev.biologists.org/lookup/doi/10.1242/dev.157917.supplemental

References

Alarcon, V. B. (2010). Cell polarity regulator PARD6B is essential for trophectoderm formation in the preimplantation mouse embryo. *Biol. Reprod.* **83**, 347-358.
Anani, S., Bhat, S., Honma-Yamanaka, N., Krawchuk, D. and Yamanaka, Y. (2014). Initiation of Hippo signaling is linked to polarity rather than to cell position in the pre-implantation mouse embryo. *Development* **141**, 2813-2824.
Berdeaux, R. L., Díaz, B., Kim, L. and Martin, G. S. (2004). Active Rho is localized to podosomes induced by oncogenic Src and is required for their assembly and function. *J. Cell Biol.* **166**, 317-323.
Cao, Z., Carey, T. S., Ganguly, A., Wilson, C. A., Paul, S. and Knott, J. G. (2015). Transcription factor AP-2gamma induces early Cdx2 expression and represses HIPPO signaling to specify the trophectoderm lineage. *Development* **142**, 1606-1615.
Chen, L., Wang, D., Wu, Z., Ma, L. and Daley, G. Q. (2010). Molecular basis of the first cell fate determination in mouse embryogenesis. *Cell Res.* **20**, 982-993.
Clayton, L., Hall, A. and Johnson, M. H. (1999). A role for Rho-like GTPases in the polarisation of mouse eight-cell blastomeres. *Dev. Biol.* **205**, 322-331.
Cockburn, K. and Rossant, J. (2010). Making the blastocyst: lessons from the mouse. *J. Clin. Invest.* **120**, 995-1003.
Cockburn, K., Biechele, S., Garner, J. and Rossant, J. (2013). The hippo pathway member nf2 is required for inner cell mass specification. *Curr. Biol.* **23**, 1195-1201.
Ernkvist, M., Aase, K., Ukomadu, C., Wohlschlegel, J., Blackman, R., Veitonmäki, N., Bratt, A., Dutta, A. and Holmgren, L. (2006). p130-angiomotin associates to actin and controls endothelial cell shape. *FEBS J.* **273**, 2000-2011.
Etienne-Manneville, S. and Hall, A. (2002). Rho GTPases in cell biology. *Nature* **420**, 629-635.
Feng, X., Degese, M. S., Iglesias-Bartolome, R., Vaque, J. P., Molinolo, A. A., Rodrigues, M., Zaidi, M. R., Ksander, B. R., Merlino, G., Sodhi, A. et al. (2014). Hippo-independent activation of YAP by the GNAQ uveal melanoma oncogene through a trio-regulated rho GTPase signaling circuitry. *Cancer Cell* **25**, 831-845.
Fleming, T. P., Mcconnell, J., Johnson, M. H. and Stevenson, B. R. (1989). Development of tight junctions de novo in the mouse early embryo: control of assembly of the tight junction-specific protein, ZO-1. *J. Cell Biol.* **108**, 1407-1418.
Hata, Y., Timalsina, S. and Maimaiti, S. (2013). Okadaic acid: a tool to study the hippo pathway. *Mar. Drugs* **11**, 896-902.
Hirate, Y., Hirahara, S., Inoue, K., Suzuki, A., Alarcon, V. B., Akimoto, K., Hirai, T., Hara, T., Adachi, M., Chida, K. et al. (2013). Polarity-dependent distribution of angiomotin localizes hippo signaling in preimplantation embryos. *Curr. Biol.* **23**, 1181-1194.
Johnson, K. C., Kissil, J. L., Fry, J. L. and Jacks, T. (2002). Cellular transformation by a FERM domain mutant of the Nf2 tumor suppressor gene. *Oncogene* **21**, 5990-5997.
Kono, K., Tamashiro, D. A. A. and Alarcon, V. B. (2014). Inhibition of RHO-ROCK signaling enhances ICM and suppresses TE characteristics through activation of Hippo signaling in the mouse blastocyst. *Dev. Biol.* **394**, 142-155.
Korotkevich, E., Niwayama, R., Courtois, A., Friese, S., Berger, N., Buchholz, F. and Hiiragi, T. (2017). The apical domain is required and sufficient for the first lineage segregation in the mouse embryo. *Dev. Cell* **40**, 235-247.e237.
Leung, C. Y. and Zernicka-Goetz, M. (2013). Angiomotin prevents pluripotent lineage differentiation in mouse embryos via Hippo pathway-dependent and -independent mechanisms. *Nat. Commun.* **4**, 2251.
Li, Y., Zhou, H., Li, F., Chan, S. W., Lin, Z., Wei, Z., Yang, Z., Guo, F., Lim, C. J., Xing, W. et al. (2015). Angiomotin binding-induced activation of Merlin/NF2 in the Hippo pathway. *Cell Res.* **25**, 801-817.
Liu, H., Wu, Z., Shi, X., Li, W., Liu, C., Wang, D., Ye, X., Liu, L., Na, J., Cheng, H. et al. (2013). Atypical PKC, regulated by Rho GTPases and Mek/Erk, phosphorylates Ezrin during eight-cell embryo compaction. *Dev. Biol.* **375**, 13-22.
Lorthongpanich, C., Messerschmidt, D. M., Chan, S. W., Hong, W., Knowles, B. B. and Solter, D. (2013). Temporal reduction of LATS kinases in the early preimplantation embryo prevents ICM lineage differentiation. *Genes Dev.* **27**, 1441-1446.
Maître, J.-L., Turlier, H., Illukkumbura, R., Eismann, B., Niwayama, R., Nédélec, F. and Hiiragi, T. (2016). Asymmetric division of contractile domains couples cell positioning and fate specification. *Nature* **536**, 344-348.
Mihajlović, A. I. and Bruce, A. W. (2016). Rho-associated protein kinase regulates subcellular localisation of Angiomotin and Hippo-signalling during preimplantation mouse embryo development. *Reprod. Biomed. Online* **33**, 381-390.
Mo, J.-S., Yu, F.-X., Gong, R., Brown, J. H. and Guan, K.-L. (2012). Regulation of the Hippo-YAP pathway by protease-activated receptors (PARs). *Genes Dev.* **26**, 2138-2143.
Nishioka, N., Yamamoto, S., Kiyonari, H., Sato, H., Sawada, A., Ota, M., Nakao, K. and Sasaki, H. (2008). Tead4 is required for specification of trophectoderm in pre-implantation mouse embryos. *Mech. Dev.* **125**, 270-283.
Nishioka, N., Inoue, K., Adachi, K., Kiyonari, H., Ota, M., Ralston, A., Yabuta, N., Hirahara, S., Stephenson, R. O., Ogonuki, N. et al. (2009). The Hippo signaling pathway components Lats and Yap pattern Tead4 activity to distinguish mouse trophectoderm from inner cell mass. *Dev. Cell* **16**, 398-410.
Pan, D. (2010). The hippo signaling pathway in development and cancer. *Dev. Cell* **19**, 491-505.
Plusa, B., Frankenberg, S., Chalmers, A., Hadjantonakis, A. K., Moore, C. A., Papalopulu, N., Papaioannou, V. E., Glover, D. M. and Zernicka-Goetz, M. (2005). Downregulation of Par3 and aPKC function directs cells towards the ICM in the preimplantation mouse embryo. *J. Cell Sci.* **118**, 505-515.
Ralston, A., Cox, B. J., Nishioka, N., Sasaki, H., Chea, E., Rugg-Gunn, P., Guo, G., Robson, P., Draper, J. S. and Rossant, J. (2010). Gata3 regulates trophoblast development downstream of Tead4 and in parallel to Cdx2. *Development* **137**, 395-403.
Sheth, B., Fesenko, I., Collins, J. E., Moran, B., Wild, A. E., Anderson, J. M. and Fleming, T. P. (1997). Tight junction assembly during mouse blastocyst formation is regulated by late expression of ZO-1 alpha+ isoform. *Development* **124**, 2027-2037.
Sheth, B., Fontaine, J.-J., Ponza, E., Mccallum, A., Page, A., Citi, S., Louvard, D., Zahraoui, A. and Fleming, T. P. (2000). Differentiation of the epithelial apical junctional complex during mouse preimplantation development: a role for rab13 in the early maturation of the tight junction. *Mech. Dev.* **97**, 93-104.
Stephenson, R. O., Yamanaka, Y. and Rossant, J. (2010). Disorganized epithelial polarity and excess trophectoderm cell fate in preimplantation embryos lacking E-cadherin. *Development* **137**, 3383-3391.
Thomas, F. C., Sheth, B., Eckert, J. J., Bazzoni, G., Dejana, E. and Fleming, T. P. (2004). Contribution of JAM-1 to epithelial differentiation and tight-junction biogenesis in the mouse preimplantation embryo. *J. Cell Sci.* **117**, 5599-5608.
Vogelsgesang, M., Pautsch, A. and Aktories, K. (2007). C3 exoenzymes, novel insights into structure and action of Rho-ADP-ribosylating toxins. *Naunyn Schmiedebergs Arch. Pharmacol.* **374**, 347-360.
Yagi, R., Kohn, M. J., Karavanova, I., Kaneko, K. J., Vullhorst, D., Depamphilis, M. L. and Buonanno, A. (2007). Transcription factor TEAD4 specifies the trophectoderm lineage at the beginning of mammalian development. *Development* **134**, 3827-3836.
Yi, C., Troutman, S., Fera, D., Stemmer-Rachamimov, A., Avila, J. L., Christian, N., Persson, N. L., Shimono, A., Speicher, D. W., Marmorstein, R. et al. (2011). A tight junction-associated Merlin-angiomotin complex mediates Merlin's regulation of mitogenic signaling and tumor suppressive functions. *Cancer Cell* **19**, 527-540.
Yin, F., Yu, J., Zheng, Y., Chen, Q., Zhang, N. and Pan, D. (2013). Spatial organization of Hippo signaling at the plasma membrane mediated by the tumor suppressor Merlin/NF2. *Cell* **154**, 1342-1355.
Yu, F.-X. and Guan, K.-L. (2013). The Hippo pathway: regulators and regulations. *Genes Dev.* **27**, 355-371.
Yu, F.-X., Zhao, B., Panupinthu, N., Jewell, J. L., Lian, I., Wang, L. H., Zhao, J., Yuan, H., Tumaneng, K., Li, H. et al. (2012). Regulation of the Hippo-YAP pathway by G-protein-coupled receptor signaling. *Cell* **150**, 780-791.
Yu, F.-X., Zhang, Y., Park, H. W., Jewell, J. L., Chen, Q., Deng, Y., Pan, D., Taylor, S. S., Lai, Z.-C. and Guan, K.-L. (2013). Protein kinase A activates the Hippo pathway to modulate cell proliferation and differentiation. *Genes Dev.* **27**, 1223-1232.
Yu, F.-X., Zhao, B. and Guan, K.-L. (2015). Hippo pathway in organ size control, tissue homeostasis, and cancer. *Cell* **163**, 811-828.
Zernicka-Goetz, M., Morris, S. A. and Bruce, A. W. (2009). Making a firm decision: multifaceted regulation of cell fate in the early mouse embryo. *Nat. Rev. Genet.* **10**, 467-477.
Zhao, B., Wei, X., Li, W., Udan, R. S., Yang, Q., Kim, J., Xie, J., Ikenoue, T., Yu, J., Li, L. et al. (2007). Inactivation of YAP oncoprotein by the Hippo pathway is involved in cell contact inhibition and tissue growth control. *Genes Dev.* **21**, 2747-2761.
Zhao, B., Li, L., Wang, L., Wang, C.-Y., Yu, J. and Guan, K.-L. (2012). Cell detachment activates the Hippo pathway via cytoskeleton reorganization to induce anoikis. *Genes Dev.* **26**, 54-68.

SUPPLEMENTARY INFORMATION

SUPPLEMENTARY FIGURES

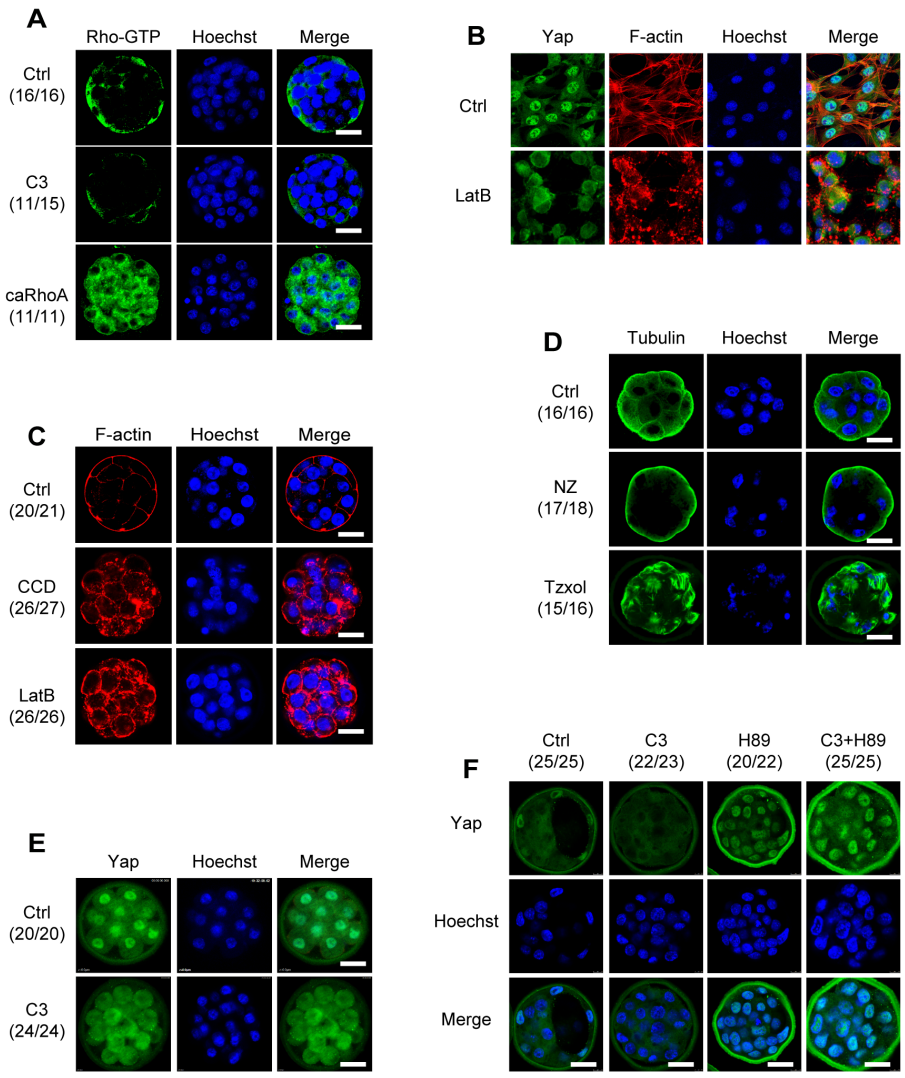

Fig. S1. Related to Fig. 2. Cell contacts, but not $G\alpha_s$-coupled GPCRs, suppress Rho signaling in ICM cells. (A) Verification of the specificity of the Rho-GTP affinity assay. Late morula / early blastocysts treated with C3 or injected with 10 ng/µl caRhoA mRNA, were subjected to Rho-GTP affinity assay. Bars: 25 µm. (B) Immunofluorescence staining of 3T3 cells treated with or without LatB for 2 hours. (C) Immunofluorescence staining of F-actin in embryos treated with CCD and LatB. (D) Immunofluorescence staining of tubulin in embryos treated with nocodazole (NZ) and taxol. Embryos were treated as described in Fig. 2C. (E) Late morula and early blastocysts were treated with calcium free medium to dissociate blastomeres, and then treated with or without C3 for 2 hours, followed by immunofluorescence analysis. (F) Late morula and early blastocysts were treated with PKA inhibitor H89 alone, Rho inhibitor C3 alone, or the combination of H89 and C3 for 2 hours, followed by immunofluorescence analysis. Bars: 25 µm.

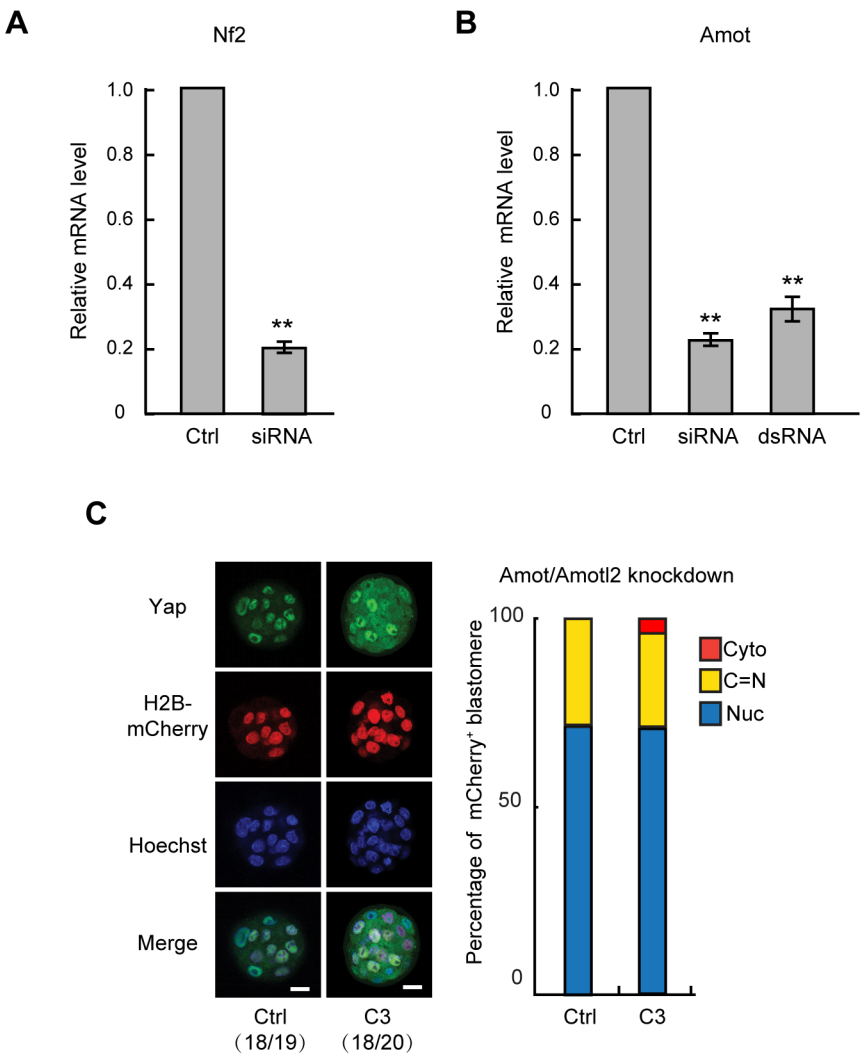

Fig. S2. Related to Fig. 3. Validation of the knockdown efficiency for *Nf2* and *Amot*, and the redundancy of Amot and Amotl2. (A) *Nf2* siRNA or negative control siRNA were transfected into embryonic stem cells. Twenty-four hours after transfection, cells were harvested. RNA was purified from these cells and subjected to quantitative RT-PCR analysis. (B) Similar to (A), except that *Amot* siRNA, *Amot* dsRNA, or negative control siRNA were transfected into embryonic stem cells. Data are shown as mean ± SD (n = 3). (C) One blastomere of the 2-cell embryo was injected with both Amot and Amotl2 siRNA, together with H2B-mCherry mRNA. At the late morula stage, embryos were treated with or without C3 for 2 hours, and fixed for immunofluorescence assay. mCherry fluorescent signals mark the progeny cells from the injected 2-cell blastomere. Left panels show the representative images. Right panel summarizes the data from about 20 embryos and more than 100 mCherry positive blastomeres.

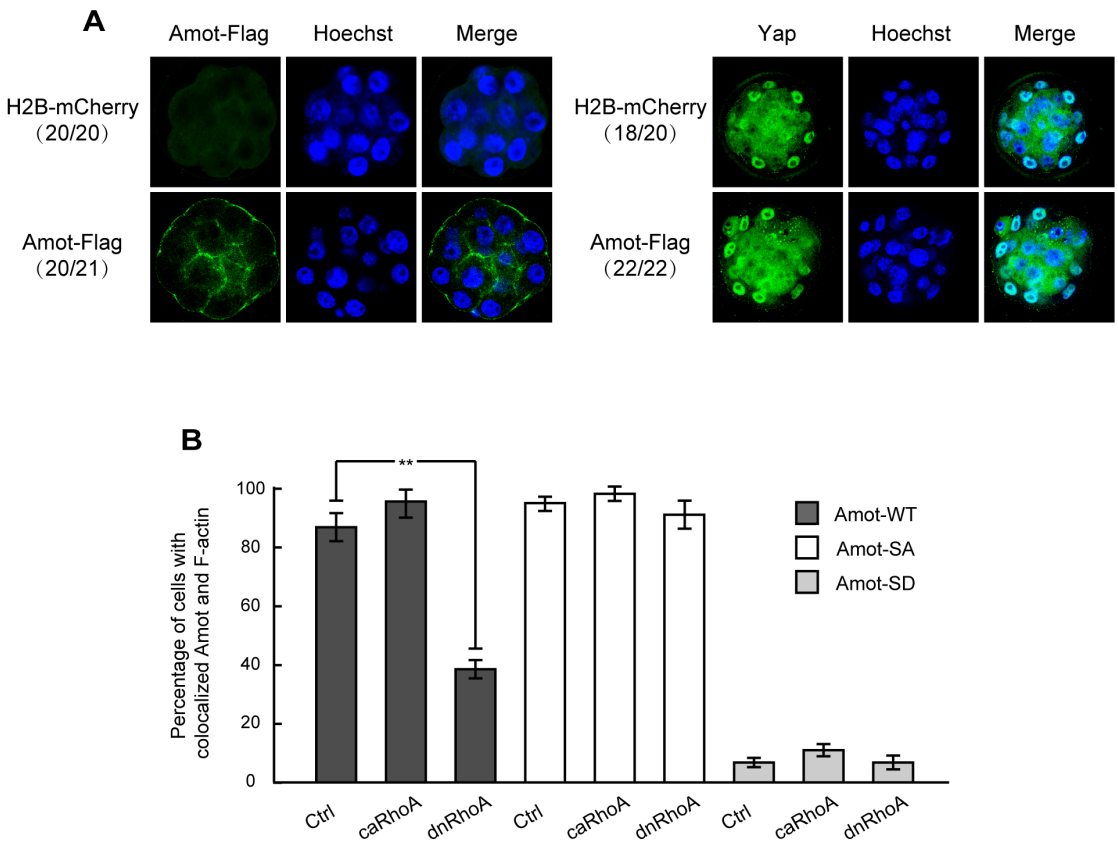

Fig. S3. Related to Fig. 4. Rho regulates the colocalization of Amot and Nf2. (A) Zygotic Amot-Flag mRNA Injection does not Yap distribution in the blastocyst. Zygotes were injected with 200 ng/µl Amot-Flag mRNA or H2B-mcherry mRNA. Blastocyst stage embryos were subject to immunofluorescence detection of Amot and Yap. Bars: 25 µm. (B) Cells with colocalized Amot and F-actin are counted from the images shown in Fig. 4C. The percentages of cells with colocalized Amot and F-actin are plotted.

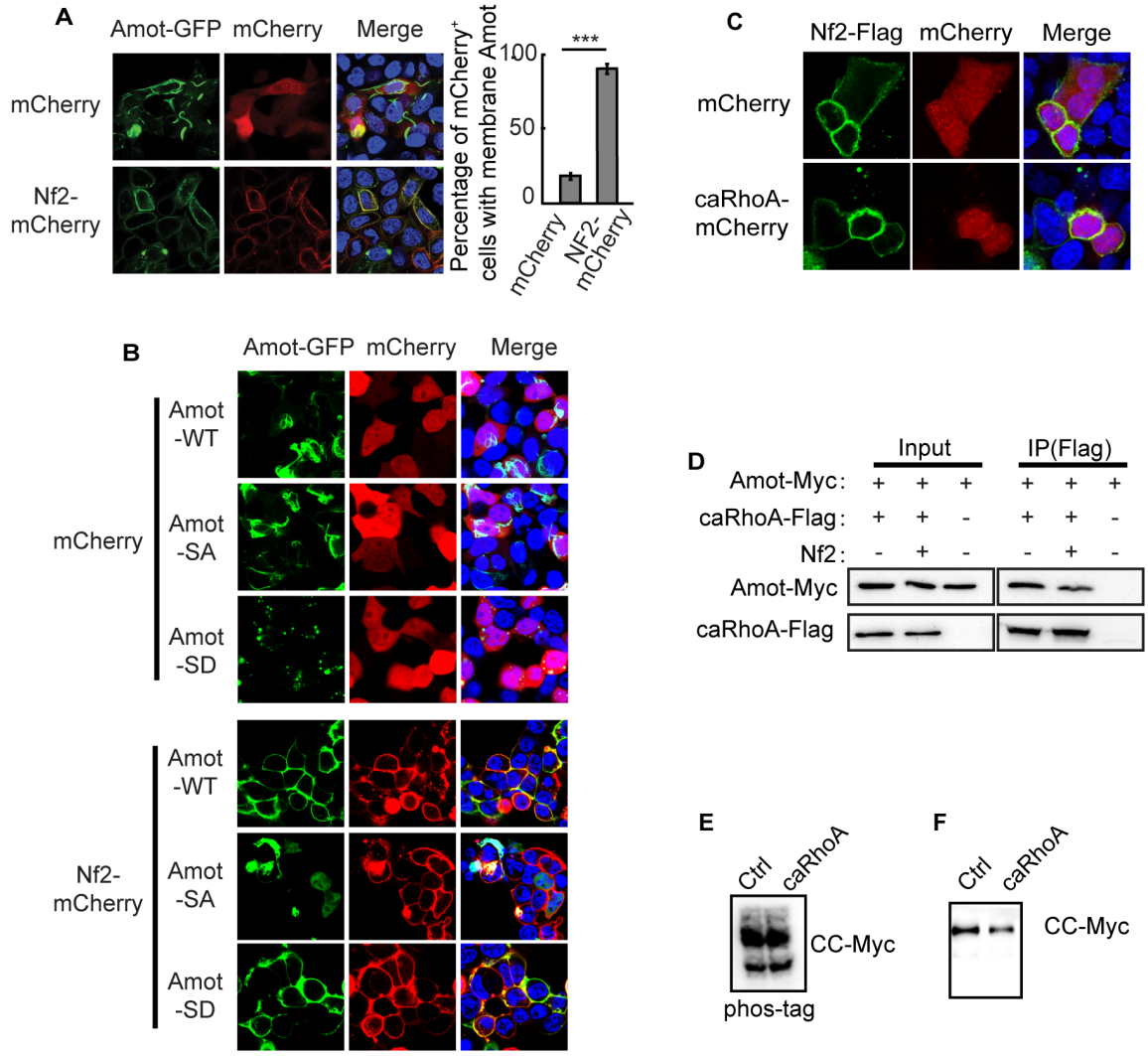

Fig. S4. Related to Fig. 5. Nf2 recruits Amot to the plasma membrane. (A) Similar to Fig. 5A, except that the experiments were carried out with Hela cells, but not with HEK293T cells. (B) GFP tagged Amot-WT, SA, and SD, were expressed, with mCherry or Nf2-mCherry, in HEK293T cells. Confocal images were taken to visualize the localization of Amot and Nf2. (C) Nf2-Flag expression vector, together with plasmids expressing mCherry or caRhoA-mCherry, was transfected into HEK293T cells. Twenty-four hours later, immunofluorescence staining with Flag antibody was performed to visualize the distribution of Nf2. mCherry signals indicate the transfected cells. (D) Plasmids expressing caRhoA-Flag and Amot-Myc, with empty or Nf2 expression vector, were co-transfected into HEK293T cells. Twenty-four hours after transfection, cells were harvested and subjected to co-IP experiment with anti-Flag M2 beads. (E-F) caRhoA does not change the electrophoretic mobility of Amot CC domain in phos-tag (E) or regular SDS-PAGE (F) gel. Plasmid expressing CC-Myc, with empty or caRhoA expression vector, was transfected into HEK293T cells. Cells were harvested at 24 hours after transfection, and cell lysates were prepared for phos-tag (E) or regular SDS-PAGE (F) electrophoresis.

SUPPLEMENTARY TABLE

Table S1. Working concentrations of inhibitors and activators

Signal Pathway	Inhibitor / activator	Working Concentration
Ras-MAPK	PD98059	1 μM
	PD0325901	1 μM
PI3K	MK2206	3 μM
RhoA-ROCK	C3 transferase	1 μg/ml
	CCG1423	10 μM
	Y27632	20 μM
PKC	D-sphingosine	2.5 μM
	GÖ 6976	1.32 μM
	Ro-31-8220	5 μM
PKA	H89	10 μM
	KT5720	5 μM
GSK3	CHIR	3 μM
GPCRs	PMA	10 ng/ml
	LPA	10 μM
	Ki16425	10 μM
PPase	Okadaic acid	0.25 μM